Extreme Mechanics Letters 4 (2015) 1–8

Contents lists available at ScienceDirect

Extreme Mechanics Letters

journal homepage: www.elsevier.com/locate/eml

Predicting fracture energies and crack-tip fields of soft tough materials

Teng Zhang [a,1], Shaoting Lin [a,1], Hyunwoo Yuk [a], Xuanhe Zhao [a,b,*]

[a] Soft Active Materials Laboratory, Department of Mechanical Engineering, Massachusetts Institute of Technology, Cambridge, MA 02139, USA

[b] Department of Civil and Environmental Engineering, Massachusetts Institute of Technology, Cambridge, MA 02139, USA

ARTICLE INFO

Article history:
Received 13 June 2015
Received in revised form 27 July 2015
Accepted 27 July 2015
Available online 30 July 2015

Keywords:
Soft materials
Fracture mechanics
Toughening

ABSTRACT

Soft materials including elastomers and gels are pervasive in biological systems and technological applications. Whereas it is known that intrinsic fracture energies of soft materials are relatively low, how the intrinsic fracture energy cooperates with mechanical dissipation in process zone to give high fracture toughness of soft materials is not well understood. In addition, it is still challenging to predict fracture energies and crack-tip strain fields of soft tough materials. Here, we report a scaling theory that accounts for synergistic effects of intrinsic fracture energies and dissipation on the toughening of soft materials. We then develop a coupled cohesive-zone and Mullins-effect model capable of quantitatively predicting fracture energies of soft tough materials and strain fields around crack tips in soft materials under large deformation. The theory and model are quantitatively validated by experiments on fracture of soft tough materials under large deformations. We further provide a general toughening diagram that can guide the design of new soft tough materials.

1. Introduction

Except bones and teeth, most parts of animal bodies consist of soft materials—elastomers and hydrogels with relatively low rigidity and high deformability compared to hard materials such as steel and ceramics. Biological soft materials such as cartilage, muscle, skin and tendon usually need to maintain high toughness, which is critical for survival and well-being of animals under various internal and external loads [1]. Soft materials also promise broad technological applications in areas as diverse as soft machines and robots [2–4], artificial tissues and organs [5], non-conventional electronics [6,7], and microfluidics and optics [8,9]. In these applications, high toughness of the materials is usually required for reliability and robust function of the systems.

Owing to their scientific and technological importance, various soft tough materials have been developed in recent decades [10–13]. The intrinsic fracture energy of soft materials – i.e., the energy required to fracture a layer of polymer chains in front of the crack [14] – is relatively low; and it is qualitatively known that the toughening of soft materials generally relies on mechanical dissipation in process zones around cracks [14–20]. However, it is still not well understood how the intrinsic fracture energy and mechanical dissipation cooperate synergistically to give rise to high fracture toughness of soft materials [21]. Furthermore, physical models that can predict the fracture energy and crack-tip strain fields of soft materials are of imminent importance to the design of new soft tough materials, but such predictive models still do not exist.

Here, we report a scaling law and a continuum model that quantitatively accounts for the synergistic contribu-

* Corresponding author at: Soft Active Materials Laboratory, Department of Mechanical Engineering, Massachusetts Institute of Technology, Cambridge, MA 02139, USA.
E-mail address: zhaox@mit.edu (X. Zhao).

[1] These authors contribute equally to this work.

http://dx.doi.org/10.1016/j.eml.2015.07.007
2352-4316/

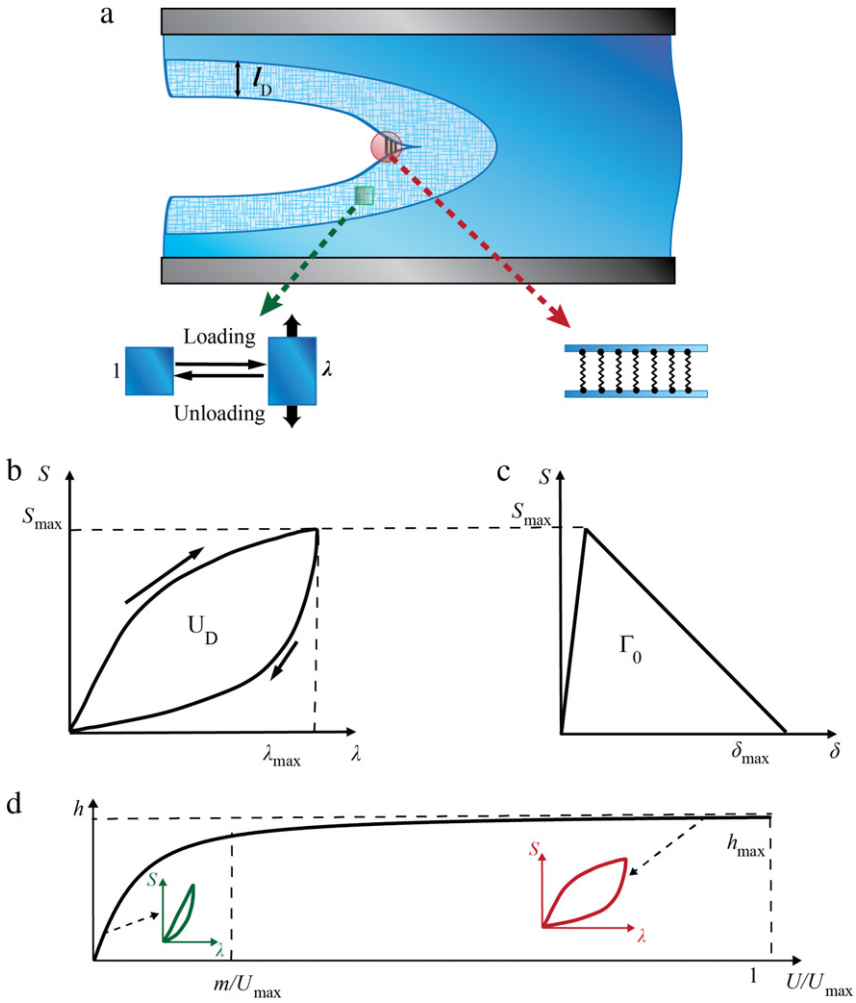

Fig. 1. Schematics of the theory and model for fracture in soft tough materials. (a) Crack propagation in a soft tough material under pure-shear test. A process zone with height l_D develops in the material during crack propagation. (b) The mechanical dissipation in the process zone is characterized by the Mullins effect. A typical stress–stretch curve of the soft material under cyclic pure-shear tensile deformation. The hysteresis loop in the curve indicates mechanical dissipation. (c) The intrinsic fracture energy of the soft material is characterized as a cohesive-zone model with triangle traction–separation law. (d) The hysteresis ratio of the soft material monotonically increases with the maximum work done to the material.

tions of intrinsic fracture energies and dissipations to the total fracture energies of soft materials. We characterize the essential physical features of intrinsic fracture energy and dissipation using the cohesive-zone model and Mullins-effect model, respectively, implemented in finite-element software, ABAQUS. Our calculation shows that the total fracture energy of soft material scales linearly with its intrinsic fracture energy, while the effect of dissipation manifests as a scaling pre-factor that can be much higher than one. To validate the theory and model, we measure the stress–strain hysteresis and intrinsic fracture energies of polyacrylamide-alginate (PAAm-alginate) hydrogels of different compositions, which represent soft tough materials with different properties [12,22]. Using the material parameters measured independently, our model can quantitatively predict the fracture energies of different soft materials as well as strain fields and crack propagations in them. Based on the model, we further calculate a toughening diagram that can guide the design of new soft tough materials.

2. Scaling analysis

Let us consider a notched soft material undergoing the pure-shear test to measure its fracture energy, as illustrated in Fig. 1(a) [23]. Crack propagation in the soft material requires the scission of at least a layer of polymer chains. The required mechanical energy for chain scission divided by the area of crack surface at undeformed state gives the intrinsic fracture energy, Γ_0. In addition, material elements in a process zone around the crack will also be deformed and undeformed as the crack propagates. If mechanical energy is dissipated during this process, the dissipated energy divided by the area of crack surface at undeformed state further contributes to the total fracture energy by, Γ_D (Fig. 1(b)). Therefore, the total fracture energy of a soft material can be expressed as

$$\Gamma = \Gamma_0 + \Gamma_D \tag{1}$$

where $\Gamma_D = \bar{U}_D l_D$ and $\bar{U}_D$ is the mechanical energy dissipated per the volume of the process zone, and l_D the

height of the process zone in the soft material at undeformed state. Since material elements in the process zone approximately undergo the pure-shear tensile deformation (i.e., tensile deformation of a thin sheet with one lateral dimension fixed as illustrated in Fig. S1(b)), we further have $\bar{U}_D \propto U_D\,(S = S_{\max})$, where U_D is the mechanical energy dissipated per unit volume of the soft material under pure-shear tensile deformation, and $S_{\max}$ is the maximum nominal stress that can be achieved in the material under pure-shear tensile deformation (Fig. 1(b)).

For a soft material represented by the neo-Hookean model in pure-shear test (Fig. 1(a)), the leading order of the nominal stress at a point near the crack tip scales as $S \propto \sqrt{2\Gamma\mu/\pi l}$ [21,24,25], where μ is the shear modulus of the materials, Γ the fracture toughness and l the distance from the point to the crack tip. Since only a region of the material around crack tip is under sufficiently high deformation (i.e., material inside the process zone) to significantly contribute to energy dissipation, we can choose a critical stress scale to determine the boundary of the process zone. It can be argued that the critical stress scale is on the same order as the maximum stress ($S_{\max}$) in the sample, and therefore the size of the process zone according to the crack tip stress field scales as

$$l_D \propto \Gamma\mu/S_{\max}^2 \propto \Gamma/U_{\max} \tag{2}$$

where $U_{\max} \propto S_{\max}^2/\mu$ is the maximum mechanical work done on the material under pure-shear tensile deformation. A combination of Eqs. (1) and (2) leads to a governing equation for the total fracture energy of soft tough materials [26–28],

$$\Gamma = \frac{\Gamma_0}{1 - \alpha \cdot h_{\max}} \tag{3}$$

where $h_{\max} = U_D\,(S = S_{\max})\,/U_{\max}$ is the ratio between the maximum dissipation and maximum mechanical work done on the material, and $0 \le \alpha \le 1$ is a dimensionless number depending on the stress–strain hysteresis of the material deformed to different levels of stresses.

3. Coupled cohesive-zone and Mullins-effect model

Next we develop a continuum model that can predict the fracture energy of soft tough materials, using material parameters measured independently. The continuum model needs to quantitatively capture the synergistic contributions of intrinsic fracture energy and mechanical dissipation in process zone to the total fracture energy. In order to model the intrinsic fracture energy of soft materials, we adopt a triangle cohesive-zone model governed by the maximum nominal stress ($S_{\max}$) and maximum nominal separation ($\delta_{\max}$) on the expected crack path (Fig. 1(c)) [24]. The damage initiation of the cohesive layer follows the quadratic nominal stress criterion

$$\left\{\frac{t_n}{S_{\max}}\right\}^2 + \left\{\frac{t_s}{S_{\max}}\right\}^2 = 1 \tag{4}$$

where $t_{(\bullet)}$ represents the nominal surface tractions on the crack surface, and the subscripts n and s indicate normal and tangential directions, respectively. When Eq. (4) is satisfied, the cohesive layer enters into the softening regime, which is described by the linear damage evolution function illustrated in Fig. 1(c). The cohesive-zone model prescribes the intrinsic fracture energy of the soft materials to be,

$$\Gamma_0 = 1/2 S_{\max}\delta_{\max}. \tag{5}$$

To physically implement the cohesive-zone model, the maximum nominal stress $S_{\max}$ of the cohesive zone is taken as the measured failure stress of the material under pure-shear tension, and the maximum nominal separation $\delta_{\max}$ is calculated based on the experimentally measured intrinsic fracture energy of the material Γ_0 and Eq. (5), i.e., $\delta_{\max} = 2\Gamma_0/S_{\max}$.

Mechanical dissipation in the process zone may arise from viscoelasticity [29,30], plasticity [31], and/or partial damage of the soft materials; and such dissipations manifest as hysteresis loops on stress–strain curves of the material (Fig. 1(b)). To capture the essential effect of dissipation in process zone on toughening, we model the dissipation as the Mullins effect in soft materials [32]. The Mullins effect gives hysteresis loops in the stress–stretch curves of the materials under loading–unloading cycles. We define the hysteresis ratio of the material under pure-shear tensile deformation as

$$h = U_D/U \tag{6}$$

where U and U_D are the mechanical work done on and the energy dissipation in a unit volume of the soft material under pure-shear tensile deformation, respectively. The hysteresis ratio of soft material generally increases with the deformation of (or the work done on) the material due to the accumulation of material damage and eventually reaches a maximum value, i.e., $h\,(S = S_{\max}) = h_{\max}$ (Fig. 1(d)), which is used in Eq. (3). To describe the Mullins effect in soft materials, we adopt the modified Ogden–Roxburgh model used in ABAQUS [33]. In brief, the free energy function of an incompressible material with Mullins effect can expressed as

$$W\,(\mathbf{F}, \eta) = \eta\tilde{W}\,(\mathbf{F}) + \phi\,(\eta) \tag{7}$$

where $\mathbf{F}$ is the deformation gradient tensor, η is a damage variable ($0 < \eta \le 1$), $\tilde{W}$ is the free energy function of a pure elastic material without Mullins effect, and $\phi\,(\eta)$ is referred to as the damage function. The damage variable η characterizes the stress softening due to material damage. The material is in its virgin state if $\eta = 1$ and fully damaged state if $\eta = 0$. The damage function and damage variable in Eq. (7) can be expressed as

$$\phi\,(\eta) = \int_1^{\eta} \left[\left(m + \beta W^m\right)\mathrm{erf}^{-1}\left(r\,(1-\eta)\right) - W^m\right] d\eta \tag{8a}$$

$$\eta = 1 - \frac{1}{r}\mathrm{erf}\left[\left(W^m - \tilde{W}\right)/\left(m + \beta W^m\right)\right] \tag{8b}$$

where W^m denotes the maximum strain energy density of the material before unloading, erf is the error function, β is a positive number to avoid overly stiff response at the initiation of unloading from relatively large stretch levels,

and r and m are constants that characterize the damage properties of the material. Throughout the calculations, we set $\beta = 0.1$ for numerical stabilization. The parameter r in Eq. (8) indicates the maximum extent of the material damage related to the virgin state [32], which therefore determines the maximum hysteresis ratio of the material under pure-shear tensile deformation, $h_{\max}$. Fig. 2(a) gives the relation between $h_{\max}$ and r for a neo-Hookean material with Mullins effect under pure-shear tensile deformation. It is evident that $h_{\max}$ is a monotonic decreasing function of r. The parameter m in Eq. (8) represents a critical energy scale that acts as a threshold for activating significant dissipation in the material. Fig. 2(b) shows the calculated hysteresis ratio h as a function of $U/U_{\max}$ for different values of $m/U_{\max}$ for a neo-Hookean material with Mullins effect under pure-shear tensile deformation. If $U/U_{\max} < m/U_{\max}$ for a material under pure-shear tensile deformation, the hysteresis ratio h is generally much smaller than $h_{\max}$, which means that the deformation of (or the work done on) the material is not sufficient to induce significant dissipation. If $U/U_{\max} \gg m/U_{\max}$, the hysteresis ratio h can reach a value close to $h_{\max}$, which means that significant dissipation has been activated. (See Fig. 1(d) for schematics and Fig. 2(c) for calculation.) Therefore, the parameter $m/U_{\max}$ indicates the speed of h increasing from 0 to $h_{\max}$ as a function of $U/U_{\max}$; a smaller value of $m/U_{\max}$ gives a faster transition to $h_{\max}$.

To physically implement the Mullins-effect model, the free energy function $\tilde{W}$ (**F**) in Eq. (6) can be obtained by fitting a hyperelastic model to the stress–stretch curve of soft material under monotonic loading. The parameters r and m in Eq. (8) can be obtained from multiple stress–stretch hysteresis of the soft material deformed to different stretches.

In order to calculate the total fracture energy and crack-tip strain field of soft material, the pure-shear test is simulated in the coupled cohesive-zone and Mullins-effect model [23] (Fig. S1 and Supplementary materials for details). In brief, two identical pieces of a soft material are clamped along their long edges with rigid plates. A notch is introduced into the first sample, which is then gradually pulled to a stretch of λ_c times of its undeformed length until a crack steadily propagates from the notch (Fig. S1(a)). Thereafter, the second sample without notch is uniformly stretched to the same critical stretch λ_c with the applied stress S recorded (Fig. S1(b)). The total fracture energy of the soft material can be calculated as $\Gamma = L_0 \int_1^{\lambda_c} S d\lambda$, where L_0 is the height of the sample shown in Fig. S1(a).

We next discuss the difference in critical stretches for crack initiation and steady-state propagation and therefore the difference in corresponding fracture energies. The crack initiation happens at the same critical stretch for a material with and without energy dissipation (i.e., with and without Mullins effect), because the unloading process and thus dissipative properties of the material do not affect crack initiation. The measured fracture energy corresponding to crack initiation reflects the intrinsic fracture energy of a material. On the other hand, the critical stretches for steady-state propagation of cracks in a material with and without energy dissipation can be very different. For pure elastic samples (i.e., without Mullins effect), the steady-state propagation of crack follows right after the crack initiation. For samples with dissipation (i.e., with Mullins effect), the steady-state propagation of crack, however, can occur at a much larger stretch than crack initiation (see Fig. S2 and supplementary movie), because the unloaded material around the crack has been softened—reflecting

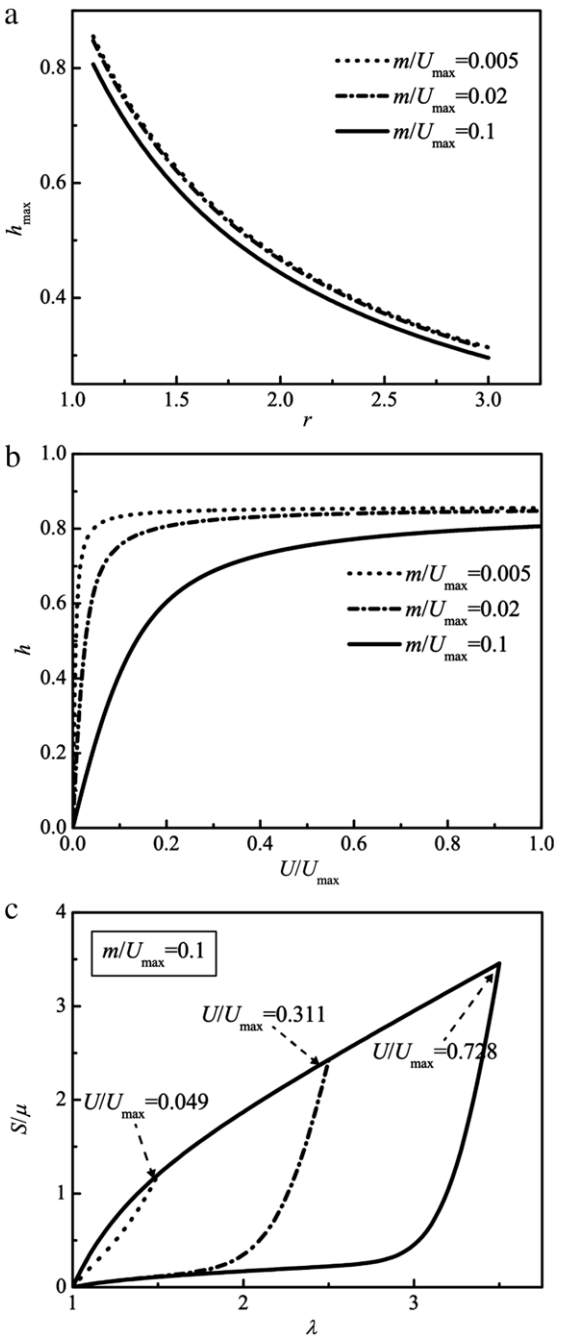

Fig. 2. The modified Ogden–Roxburgh model for Mullins effect. (a) The relation between $h_{\max}$ and r for a neo-Hookean material with Mullins effect under pure-shear tensile deformation. (b) The calculated h as a function of $U/U_{\max}$ for different values of $m/U_{\max}$ for a neo-Hookean material with Mullins effect under pure-shear tensile deformation. (c) The calculated stress–stretch hysteresis for a neo-Hookean material with Mullins effect under pure-shear tensile deformation.

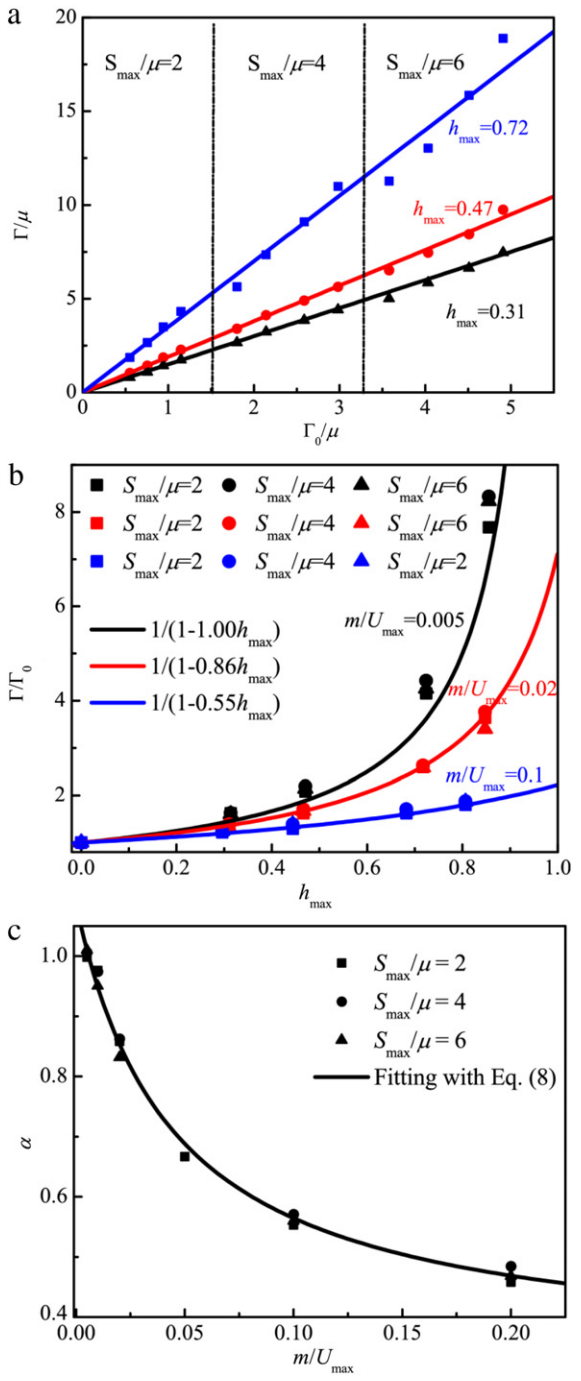

Fig. 3. Calculated fracture energies of soft materials from the coupled cohesive-zone and Mullins-effect model. (a) Calculated Γ as a function of Γ_0 for soft materials with different S_{max}/μ and h_{max}. The value of m/U_{max} is set to be 0.01. (b) Calculated Γ as a function of h_{max} for soft materials with various values of S_{max}/μ and m/U_{max}. (c) Calculated parameter α in Eq. (3) as a function of m/U_{max}.

the toughening effect of mechanical dissipation. In the current study, we use the fracture energy measured at steady-state propagation of crack (i.e., the steady-state critical energy release rate G^{ss}) to give the total fracture energy Γ of materials with and without dissipation.

4. Theoretical and numerical results

Next, we will use the coupled cohesive-zone and Mullins-effect model to validate the scaling for total fracture energies of soft materials. The soft material under loading is taken as a neo-Hookean material with initial shear modulus μ. Based on the coupled cohesive-zone and Mullins effect model, the total fracture energy of the soft material, Γ, is mainly determined by a set of four parameters including μ, Γ_0, h_{max}, S_{max}, and m/U_{max}. (Note that U_{max} is approximately equal to $S_{max}^2/2\mu$ for neo-Hookean materials.) We will vary these parameters independently in the model, and calculate the fracture energy of the materials following the pure-shear method described above. Without loss of generality, we use the initial shear modulus μ to normalize S_{max}, Γ_0 and Γ. In Fig. 3(a), the calculated values of Γ are plotted as functions of Γ_0 of materials with different combinations of S_{max}/μ and h_{max}. It can be seen that Γ is linearly scaled with Γ_0 in all the calculated cases. With this knowledge in mind, we next explore the enhanced ratio of the fracture energy (Γ/Γ_0) due to mechanical dissipation in the process zone. We calculate Γ/Γ_0 as functions of h_{max} for various combinations of S_{max}/μ and m/U_{max}. Fig. 3(b) shows that the relation $\Gamma/\Gamma_0 = 1/(1-\alpha\cdot h_{max})$ is valid for wide ranges of S_{max}/μ (i.e., from 2 to 6) and m/U_{max} (i.e., 0.005–0.1). In addition, it can be seen that the calculated values of Γ/Γ_0 from models with different S_{max}/μ but the same m/U_{max} are approximately the same. This means the parameter α in Eq. (4) mainly depends on the normalized critical energy scale, m/U_{max}. In Fig. 3(c), we summarize the calculated parameter α as a function of m/U_{max} for different values of S_{max}/μ. It is evident that α does not depend on S_{max}/μ, which is consistent with the result in Fig. 3(b). In addition, α is a monotonic decreasing function of m/U_{max}. This trend can be qualitatively understood as follow. When the normalized work done on a material element in the process zone exceeds a critical value m/U_{max}, the element begins to dissipate mechanical energy significantly. Therefore, for materials with otherwise the same properties, a lower value of m/U_{max} gives more dissipation in the process zone and thus a higher enhancement of the fracture energy, i.e., higher value of Γ/Γ_0. Based on the models' results (Fig. 3(c)), we further fit α as a function of m/U_{max} for neo-Hookean materials as

$$\alpha \approx 0.33 + \frac{0.034}{m/U_{max} + 0.045}. \tag{9}$$

Based on Eqs. (3) and (9), we summarize the toughness enhancement of soft materials, Γ/Γ_0, as a function of the maximum hysteresis ratio h_{max} and the normalized critical energy scale for significant dissipation m/U_{max} in Fig. 4. The results reveal three critical factors in toughening of soft materials: (1) high intrinsic fracture energy (i.e., high Γ_0), (2) high value of maximum hysteresis ratio (i.e., high h_{max}), and (3) quick transition to the maximum hysteresis (i.e., low m/U_{max}). These findings are consistent with the underlying physical mechanisms for the design of soft tough materials, such as large amounts of long stretchy polymer chains for high intrinsic fracture energy, sacrificial bonds for high energy dissipation, and high stretchability for a

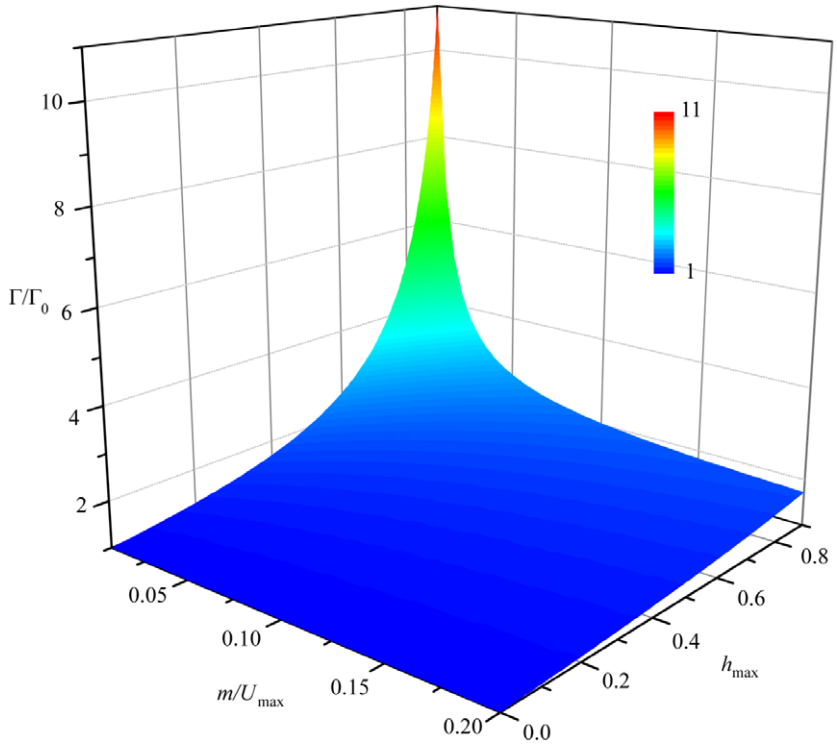

Fig. 4. A quantitative diagram for toughening mechanisms of soft materials. The toughness enhancement ratio Γ/Γ_0 as a function of $h_{\max}$ and $m/U_{\max}$, calculated based on Eqs. (3) and (9).

quick transition from zero to maximum hysteresis ratio. Our theoretical models can quantify the contributions from each factor, and therefore provide quantitative guidelines for the design of future soft tough materials.

5. Experimental validation

To validate the proposed theory and model, we take the interpenetrating-network hydrogel of polyacrylamide-alginate as a model soft tough material. (Details of the material synthesis are given in the supplementary materials.) We measure stress–stretch curves and various hysteresis ratios of the hydrogel under pure-shear tensile deformation up to the maximum stress $S_{\max}$, and then implement the measured data into the modified Ogden–Roxburgh model in ABAQUS. As shown in Fig. 5(a), the pure elastic deformation of the hydrogel (sample 1) can be well described by the Ogden hyperelastic model [34]. In Fig. 5(b), we compare the measured hysteresis ratio of the hydrogel under different deformation (i.e., different $U/U_{\max}$) with the model's prediction, validating that the Ogden–Roxburgh model can accurately characterize the dissipative property of the hydrogel. In order to measure the intrinsic fracture energy of the hydrogel, we pre-deform the hydrogel samples to a level of stress approximately $S_{\max}$ for multiple cycles to deplete the dissipative capacity of the samples [12,22]. Thereafter, the pure-shear test is used to measure the stress–stretch hysteresis and fracture energy of the pre-deformed sample. There is almost no stress–stretch hysteresis of the sample pre-deformed to $S_{\max}$ [22], indicating negligible mechanical dissipation of the sample. In addition, the measured fracture energy as a function of pre-deformation indeed reaches an asymptote (Fig. 5(c)), which gives the intrinsic fracture energy of the hydrogel without the effect of dissipation in the process zone. The measured intrinsic energy is then implemented through the cohesive-zone model in ABAQUS.

Now that the material parameters of the hydrogel have been independently measured and implemented in the continuum model, we will perform the pure-shear tests on samples both in experiments and in the model to obtain the fracture energies of the hydrogel. The samples are chosen large enough to avoid the finite specimen size effect on the measured fracture energies [12]. (Details of the sample geometry are given in the supplementary materials.) It should be noted that, in other studies, the process zone can be as large as the tested sample, making the fracture toughness as an extrinsic quantity depending on the specimen size [20]. In Fig. 5(d), we compare the force–displacement curves of the notched sample from experiment and calculation, and find that the theoretically predicted curve and critical point for steady-state crack propagation are in good agreement with experimental results. We further use digital image correlation (DIC) method (see details in Fig. S4) to measure the strain field around the notch in the sample under pure-shear test. As shown in Fig. 5(e)–(f) and the supplementary movie, the strain fields around the notch predicted by the model are consistent with the measured results by DIC. One of the advantages of our numerical simulations is to visualize the distribution of the exact amount of the energy dissipation in the materials,

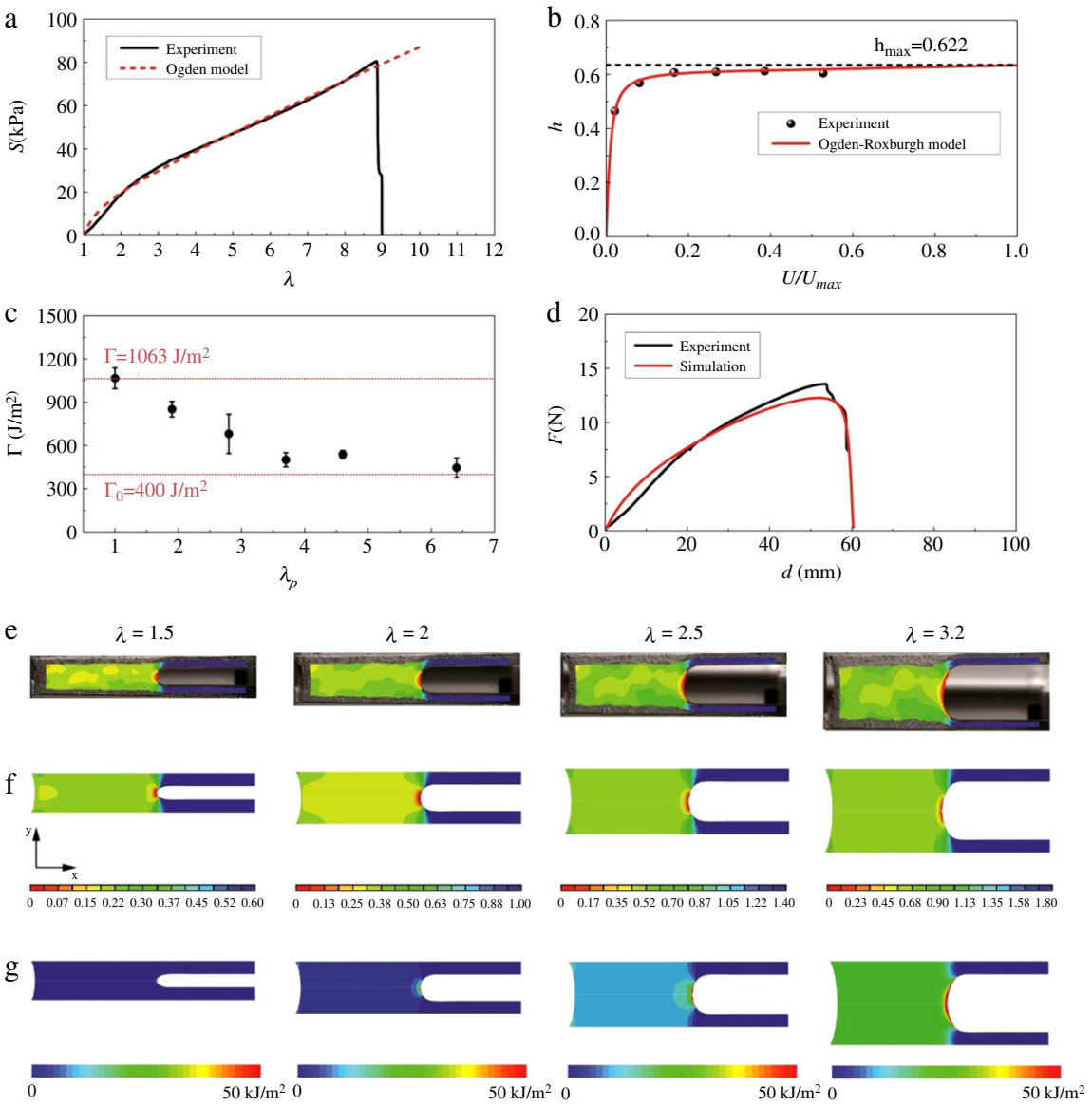

Fig. 5. Comparison between experiments and simulations on fracture of PAAm-alginate hydrogel Sample 1. (a) Stress–stretch curve of the sample under pure-shear tensile deformation and one term Ogden model, i.e., $\tilde{W} = 2\mu/\alpha_1^2\left(\lambda_1^{\alpha_1} + \lambda_2^{\alpha_1} + \lambda_3^{\alpha_1} - 3\right)$, with $\mu = 10.81$ kPa and $\alpha_1 = 1.879$. (b) The measured hysteresis ratios of the material deformed to different stretches, and the calculated hysteresis ratio by the modified Ogden–Roxburgh model with $r = 1.516$ and $m = 4.274\ \mathrm{J/m^3}$. (c) Measured fracture energy of the sample pre-deformed to different pre-stretches λ_p. (d) Force–displacement curves of the notched sample under pure-shear test measured from the experiment and predicted by the model. The strain field in the notched sample under pure-shear test to different stretches: (e) measured by DIC in the experiment and (f) predicted by the model. (g) Energy dissipated in the notched sample under pure-shear test to different stretches. The color represents the true strain (ε_{yy}) in (e) and (f) and the density of the energy dissipation in (g). (For interpretation of the references to color in this figure legend, the reader is referred to the web version of this article.)

while it is extremely challenging to obtain such quantitative data experimentally [13,35]. From Fig. 5(g), it can be seen that a region of significant dissipation indeed encapsulates the crack tip, and the area of the region gradually increases with the external load until crack propagation. To further validate the predictive capability of the model, we fabricate another polyacrylamide-alginate hydrogel with a different composition and therefore different mechanical properties, referred to as sample 2. We then perform the same pure-shear experiment and simulation on sample 2, and show that the experiment and simulation results agree well with each other (see details in Fig. S5).

6. Conclusion

In this paper, we propose a scaling law that accounts for synergistic effects of intrinsic fracture energies and mechanical dissipations on the toughening of soft materials. We then develop a coupled cohesive-zone and Mullins effect model to quantitatively predict the fracture energies and crack-tip strain fields in soft tough materials, using

material parameters measured independently. The theory and the model show that the toughening of a soft material relies on high intrinsic fracture energy of the material, high value of maximum hysteresis ratio of the material, and quick transition to the maximum hysteresis in the material under deformation. We further perform pure-shear experiments coupled with DIC on tough hydrogels to measure their fracture energies and strain fields around crack tips, and show that the experimental results match well with the model's predictions. The theory and model can provide quantitative guidance for the design of future soft tough materials.

Acknowledgments

The authors acknowledge Prof. Lallit Anand for helpful discussions on cohesive-zone model. The work is supported by ONR (No. N00014-14-1-0528) and MIT Institute of Soldier Nanotechnology. The authors are also grateful for the support from MIT research computing resources.

Appendix A. Supplementary data

Supplementary material related to this article can be found online at http://dx.doi.org/10.1016/j.eml.2015.07.007.

References

[1] N. Simha, C. Carlson, J. Lewis, J. Mater. Sci. Mater. Med. 15 (2004) 631.
[2] S.A. Morin, R.F. Shepherd, S.W. Kwok, A.A. Stokes, A. Nemiroski, G.M. Whitesides, Science 337 (2012) 828.
[3] Z. Suo, MRS Bull. 37 (2012) 218.
[4] H. Gao, X. Wang, H. Yao, S. Gorb, E. Arzt, Mech. Mater. 37 (2005) 275.
[5] K.Y. Lee, D.J. Mooney, Chem. Rev. 101 (2001) 1869.
[6] J.A. Rogers, T. Someya, Y. Huang, Science 327 (2010) 1603.
[7] C. Yu, et al., Adv. Mater. 25 (2013) 1541.
[8] S.R. Quake, A. Scherer, Science 290 (2000) 1536.
[9] S.R. Sershen, G.A. Mensing, M. Ng, N.J. Halas, D.J. Beebe, J.L. West, Adv. Mater. 17 (2005) 1366.
[10] J.P. Gong, Y. Katsuyama, T. Kurokawa, Y. Osada, Adv. Mater. 15 (2003) 1155.
[11] K.J. Henderson, T.C. Zhou, K.J. Otim, K.R. Shull, Macromolecules 43 (2010) 6193.
[12] J.-Y. Sun, X. Zhao, W.R. Illeperuma, O. Chaudhuri, K.H. Oh, D.J. Mooney, J.J. Vlassak, Z. Suo, Nature 489 (2012) 133.
[13] E. Ducrot, Y. Chen, M. Bulters, R.P. Sijbesma, C. Creton, Science 344 (2014) 186.
[14] G. Lake, A. Thomas, Proc. R. Soc. Lond. Ser. A Math. Phys. Sci. 300 (1967) 108.
[15] H.R. Brown, Macromolecules 40 (2007) 3815.
[16] R.E. Webber, C. Creton, H.R. Brown, J.P. Gong, Macromolecules 40 (2007) 2919.
[17] Y. Tanaka, Europhys. Lett. 78 (2007) 56005.
[18] J.P. Gong, Soft Matter 6 (2010) 2583.
[19] X. Zhao, Soft Matter 10 (2014) 672.
[20] B. Liu, Y. Jia, H.L. Wang, H. Gao, 2015. arXiv:0905.1855v2.
[21] R. Long, C.-Y. Hui, Extreme Mech. Lett. (2015).
[22] S. Lin, Y. Zhou, X. Zhao, Extreme Mech. Lett. 1 (2014) 70.
[23] R. Rivlin, A.G. Thomas, J. Polym. Sci. 10 (1953) 291.
[24] C.-Y. Hui, A. Jagota, S. Bennison, J. Londono, Proc. R. Soc. Lond. Ser. A Math. Phys. Eng. Sci. 459 (2003) 1489.
[25] V.R. Krishnan, C.Y. Hui, R. Long, Langmuir 24 (2008) 14245.
[26] R. McMeeking, A. Evans, J. Am. Ceram. Soc. 65 (1982) 242.
[27] B. Budiansky, J. Hutchinson, J. Lambropoulos, Internat. J. Solids Structures 19 (1983) 337.
[28] A.G. Evans, Z. Ahmad, D. Gilbert, P. Beaumont, Acta Metall. 34 (1986) 79.
[29] T. Baumberger, C. Caroli, D. Martina, Nat. Mater. 5 (2006) 552.
[30] T. Nguyen, S. Govindjee, Int. J. Fract. 141 (2006) 255.
[31] T.L. Sun, T. Kurokawa, S. Kuroda, A.B. Ihsan, T. Akasaki, K. Sato, M.A. Haque, T. Nakajima, J.P. Gong, Nat. Mater. 12 (2013) 932.
[32] R. Ogden, D. Roxburgh, Proc. R. Soc. Lond. Ser. A Math. Phys. Eng. Sci. 455 (1999) 2861.
[33] D. Systèmes, Simulia Corp. Providence, RI, USA, 2007.
[34] R.W. Ogden, Non-Linear Elastic Deformations, Courier Dover Publications, 1997.
[35] Q. Wang, G.R. Gossweiler, S.L. Craig, X. Zhao, J. Mech. Phys. Solids 82 (2015) 320.

Supplementary Materials for

Predicting Fracture Energies and Crack-Tip Fields of Soft Tough Materials

Teng Zhang[1,a)], Shaoting Lin[1,a)], Hyunwoo Yuk[1], Xuanhe Zhao[1,2, b)]

[1.] *Soft Active Materials Laboratory, Department of Mechanical Engineering, Massachusetts Institute of Technology, Cambridge, MA 02139, USA;* [2.] *Department of Civil and Environmental Engineering, Massachusetts Institute of Technology, Cambridge, MA 02139, USA*

a) These authors contribute equally to this work

b) To whom correspondence should be addressed. Email: zhaox@mit.edu

Pure-shear test for the measurement of fracture energy

To measure the fracture energy of the samples, we separately stretch two identical samples with the same thickness T_0, width W_0 and initial gage length L_0, where $W_0 >> L_0 >> T_0$ (see **Fig. S1**). One sample is notched with a crack length ranging from $0.25W_0$ to $0.5W_0$ and the other is un-notched. The notched sample is stretched to a critical distance L_c until crack starts to propagate while the un-notched sample is stretched to measure the force-displacement curve. The fracture energy of the gel can be calculated by $\Gamma = \int_{L_0}^{L_c} Fdl \Big/ \left(W_0 T_0\right)$ [1].

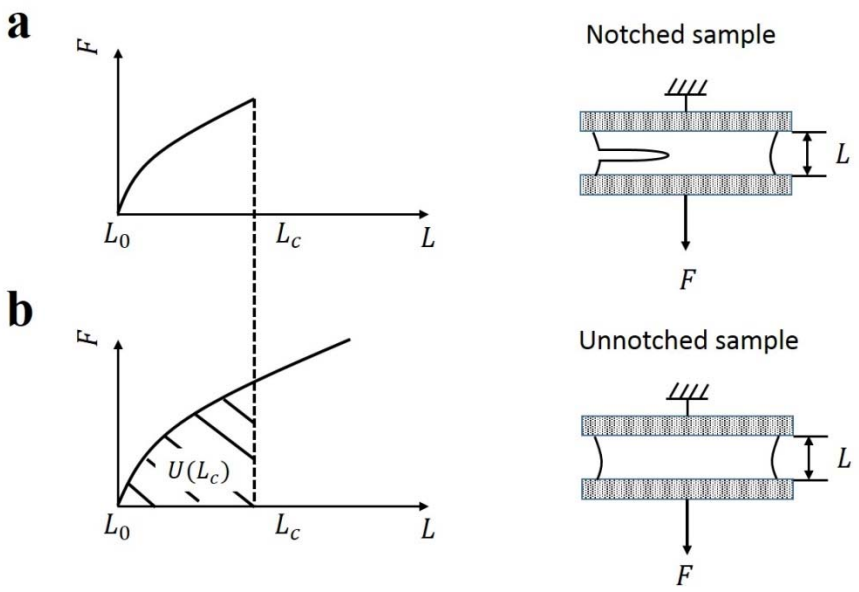

Figure S1. **Schematic of pure-shear test for measuring fracture energy of hydrogels**. (a) Notched samples are stretched to critical distance of L_c until the crack propagates. (b) Un-notched samples are stretched to L_c with the force F recorded and the fracture energy of the hydrogel can be calculated as $\Gamma = (\int_{L_0}^{L_c} F dl)/(W_0 T_0)$, where W_0, T_0 and L_0 represents width, thickness and initial gage length of the sample, respectively.

Finite-element models

We implemented the coupled cohesive-zone and Mullins-effect model into a two-dimensional (2D) finite-element model to simulate the pure-shear test of soft materials. As shown in **Fig. S2**, the numerical model consists of a finite strip with a height of L_0, width of W_0

and an initial crack length of a. The geometry of the simulated strip is taken as L_0=60 mm, W_0=480 mm, and a =120 mm unless otherwise specified. The pure elastic properties the hydrogel were modeled as the one term Ogden hyperelastic material [2]

$$\tilde{W} = 2\mu/\alpha_1^2\left(\lambda_1^{\alpha_1} + \lambda_2^{\alpha_1} + \lambda_3^{\alpha_1} - 3\right) \tag{S1}$$

where μ is the shear modulus, α_1 a fitting parameter and λ_i the i_{th} principle stretch (i=1,2,3). A Neo-Hookean material model (i.e., $\alpha_1 = 2$) is first adopted as the model material to gain theoretical understanding of the toughness enhancement due to energy dissipation. Also, it has been shown that Eq. (S1) can accurately capture the elastic deformation of the hydrogels used in current study (**Fig. 5a** and **Fig. S5**).

All the finite-element calculations are performed with ABAQUS/Explicit. Since the explicit simulations cannot handle fully incompressible materials, we set the Poisson's ratio of the soft materials to be larger than 0.499. The soft material is modeled using plane-stress 4-node linear elements with reduced integration (CPS4R). The cohesive interaction for describing crack propagation is described with the cohesive element implemented in ABAQUS (COH2D). The crack surface is uniformly discretized with very fine mesh (0.1 mm). The hydrogel strip is loaded by fixing the displacement along horizontal direction of the top and bottom surfaces and moving them along vertical direction with a constant velocity. A very low loading rate is adopted to ensure a quasistatic process, which can be verified by the stress-stretch curves from simulations under different loading rates (**Fig. S2a**). The maximum stress point on the stress-stretch curve is used to calculate the fracture energy according to the pure-shear method described above. As shown in **Fig. S2b-c**, the failures of the materials with and without the Mullins effect occur at critical stretch ratios around 1.24 and 1.07, respectively, corresponding to an order magnitude enhancement in fracture energy.

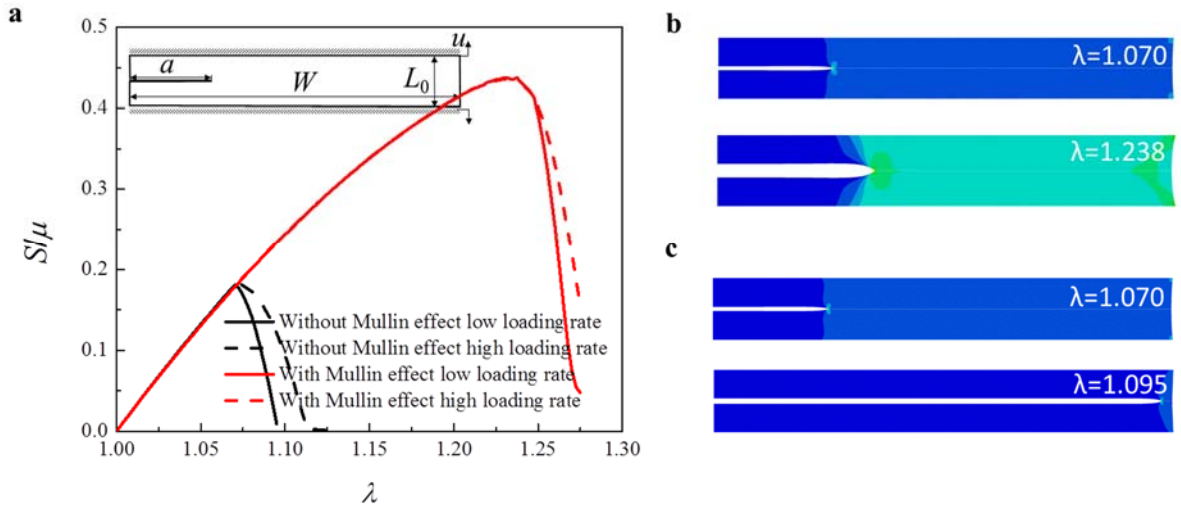

Figure S2. **Numerical simulations for the toughening effect of energy dissipation**. (a) Stress-stretch curves for materials with and without Mullins effect. The inset figure is the schematic show of the simulated model. (b) Snapshots for the crack initiation and propagation in the materials with Mullins effect (h_{max}=0.858). The crack initiates at the stretch level of 1.07, but does not propagate until the stretch level of 1.24 due to the effect of mechanical energy dissipation. (c) Snapshots for the crack initiation and propagation in the materials without Mullins effect. The crack initiates and propagates at the stretch level of 1.07.

We next validate the choices of the stiffness of the cohesive zone k and mesh size used in the simulations. The simulated sample contains 70,000 elements when using minimum mesh size as 0.1 mm. It is very difficult to further reduce the mesh size with the current available computational resources for us. We thus choose a smaller sample (L_0=20 mm, W_0=160 mm, and a =40 mm) for the validation. As demonstrated in **Fig. S3a**, the stress-stretch curves converge to

a single curve for large enough stiffness of the cohesive zone (i.e., $k/S_{max} > 15$). Therefore, we set the stiffness of cohesive zone k is always at least 15 times larger than S_{max} in the simulations to eliminate the influence of the cohesive layer on the mechanical response of the materials. As shown in **Fig. S3b**, simulations with two different mesh sizes (0.1 and 0.05 mm) are in good agreement with each other, indicating that our results are insensitive to the mesh size (0.1 mm) adopted in current simulations.

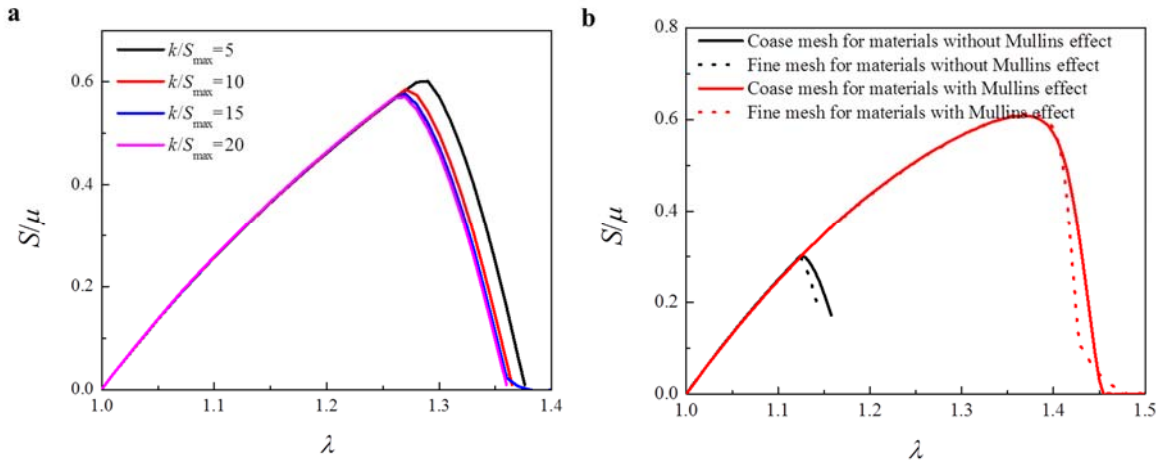

Figure S3. **Validation of the finite element models**. (a) Effect of the stiffness value of the cohesive zone k on the simulations. (b) Effect of mesh size on the simulations.

Material preparation and mechanical test

To validate the proposed theory and model, we take the interpenetrating-network hydrogel of PAAm-Alginate as a model material to investigate the toughness enhancement due to energy dissipation in a realistic soft material. A pre-gel solution is prepared by mixing 4.1 mL 4.8 wt% alginate (Sigma, A2033) and 5.5 mL 18.7 wt% acrylamide (Sigma, A8887). We add 900 μL

0.2g/100ml N,N-methylenebisacrylamide (Sigma, 146072) as the crosslinker for polyacrylamide and 102 µL 0.2 M ammonium persulphate (Sigma, 248614) as a photo initiator for polyacrylamide. After degassing the pre-gel solution in a vacuum chamber, we add respectively 200 µL and 300 µL (sample 1: 200 µL; sample 2: 300 µL) 1 M calcium sulphate (Sigma, C3771) as the crosslinker for alginate and 8.2 µL N,N,N',N'-tetramethylethylenediamine (Sigma, T7024-50M) as the crosslinking accelerator for polyacrylamide to form hydrogels with different energy dissipation. Thereafter, the pre-gel solution is infused into a glass mold and is subjected to ultraviolet light for 60 minutes with 8 W power and 254 nm wavelength to cure the hydrogel. Pure-shear tension test is applied on the samples with Zwick/Roell Z2.5 materials testing machine at room temperature. The hydrogel strip for experimentally measuring the fracture energy has a dimension of L_0=20 mm, W_0=180 mm and a =90 mm, which also applies to the numerical simulations presented in **Fig. 5** and **Fig. S5**. As demonstrated by previous study [3], the current size is large enough to obtain fracture energies that are independent of the specimen size.

Digital image correlation

As illustrated by **Fig. S4**, digital image correlation is a non-contact optical technique that allows full-field strain measurement on a surface under deformation [4]. A random speckle pattern is generated on the surface of a sample by spray painting. Images of speckle patterns at both reference state and deformed state were recorded by a standard video camera during the process of the deformation. Both images are transformed to grey matrices. To track the surface displacements of deforming materials, a mathematically well-defined correlated function is applied to match digitalized images before deformation and after deformation [5]

$$r(x,y)=1-\frac{\sum A(x,y)B(x^*,y^*)}{(\sum A(x,y)^2 * \sum B(x^*,y^*)^2)^{1/2}}, \tag{S2}$$

where $A(x,y)$ is the grey level at the location of (x,y) at reference state, $B(x^*,y^*)$ represents the grey level at the location of (x^*,y^*) at deformed state. The relation between (x^*,y^*) and (x,y) can be related as:

$$\begin{cases} x^* = x + u + \dfrac{\partial u}{\partial x}\Delta x + \dfrac{\partial u}{\partial y}\Delta y \\ y^* = y + v + \dfrac{\partial v}{\partial x}\Delta x + \dfrac{\partial v}{\partial y}\Delta y \end{cases}, \tag{S3}$$

where u and v respectively represents the displacements in the direction of x and y .The displacements can be determined by minimizing the correlated function $r(x,y)$.

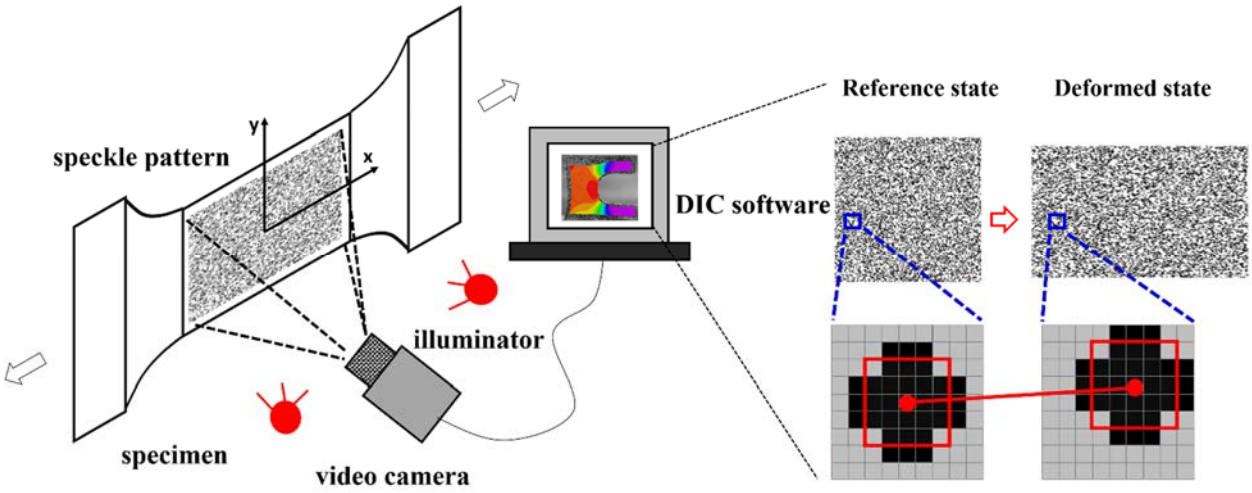

Figure S4. **Schematic of digital image correlation technique**. A random speckle pattern is spray painted onto the surface of a sample. Images of the speckle patterns at both the reference state and deformed state are recorded by a standard video camera throughout sample extension.

The surface strain is measured by matching the digitalized images before and after deformation via VIC-2D software.

Experimental validation with hydrogel sample 2

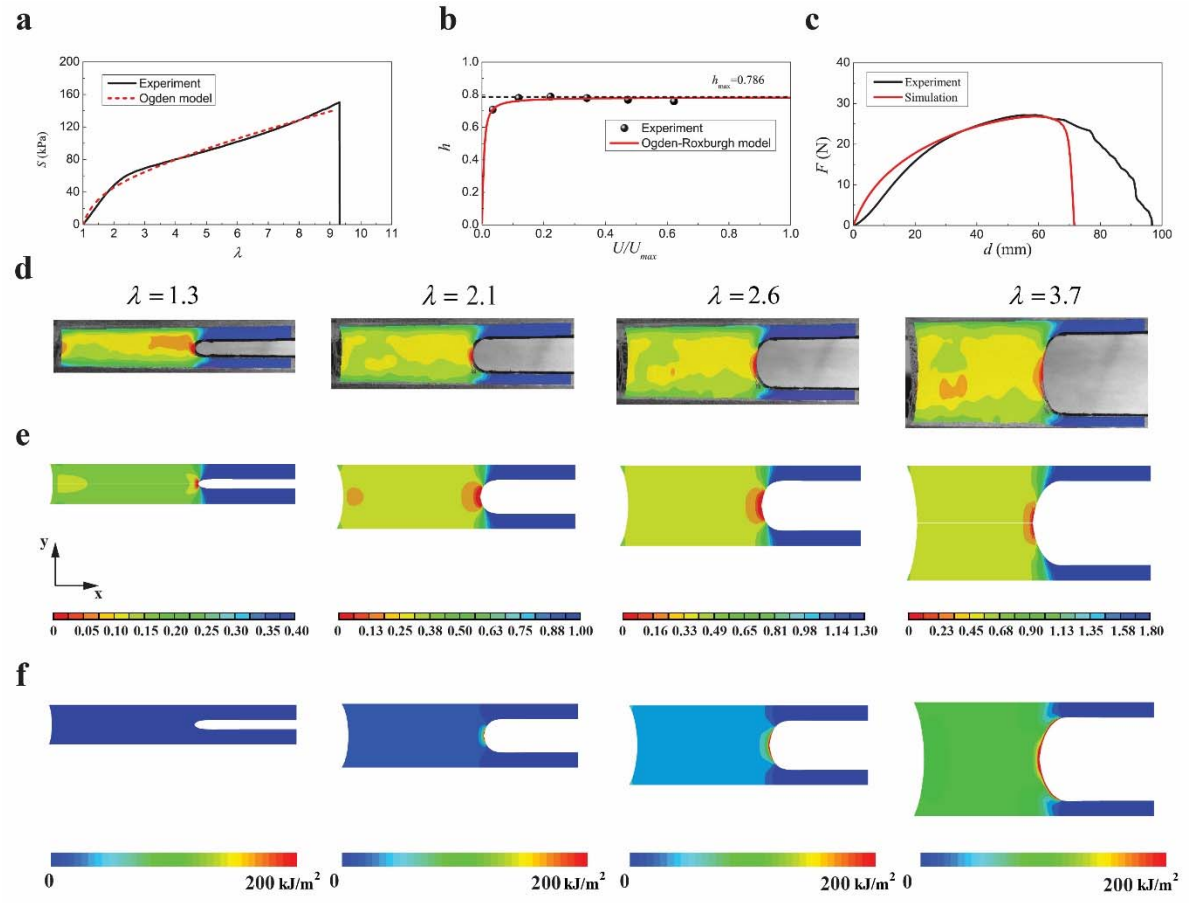

Figure S5. **Comparison between experiments and simulations on fracture of PAAm-alginate hydrogel Sample 2.** (a) Stress-stretch curves of the sample under pure-shear tensile deformation and one term Ogden model, i.e., $\widetilde{W} = 2\mu/\alpha_1^2\left(\lambda_1^{\alpha_1} + \lambda_2^{\alpha_1} + \lambda_3^{\alpha_1} - 3\right)$, with μ = 26.49 kPa and α_1 = 1.674. (b) The measured hysteresis ratios of the material deformed to different stretches, and the calculated hysteresis ratio by the modified Ogden-Roxburgh model with r=1.203 and m=4.119 J/m^3. (c) Force-displacement curves of the notched sample under pure-shear test

measured from the experiment and predicted by the model. The strain field in the notched sample under pure-shear test to different stretches: (d) measured by DIC in the experiment and (e) predicted by the model. (f) Energy dissipated in the notched sample under pure-shear test to different stretches. The color represents the true strain (ε_{yy}) in (d) and (e) and the density of the energy dissipation in (f).

Supplementary movie. Comparison between experiments and simulations on fracture of PAAm-alginate hydrogel Sample 1. The counter represents the true strain (ε_{yy}).

Additional Reference

[1] R. Rivlin and A. G. Thomas, Journal of polymer Science **10**, 291 (1953).
[2] R. W. Ogden, *Non-linear elastic deformations* (Courier Dover Publications, 1997).
[3] J.-Y. Sun, X. Zhao, W. R. Illeperuma, O. Chaudhuri, K. H. Oh, D. J. Mooney, J. J. Vlassak, and Z. Suo, Nature **489**, 133 (2012).
[4] W. Peters and W. Ranson, Optical Engineering **21**, 213427 (1982).
[5] H. Bruck, S. McNeill, M. A. Sutton, and W. Peters Iii, Experimental Mechanics **29**, 261 (1989).